

paper 6

 [Composite Structures 276 \(2021\) 114568](#)

Contents lists available at [ScienceDirect](#)

Composite Structures

journal homepage: www.elsevier.com/locate/compstruct

Experimental testing of novel hybrid rubberised concrete double skin 
tubular columns with filament wound CFRP tube under axial compressive
loading

**Shovona Khusru a, David P.
Thambiratnam a, Mohamed
Elchalakani b, Sabrina Fawzia a,***

a School of Civil and Environmental Engineering, Science and Engineering
Faculty, Queensland University of Technology, Australia b Department of
Civil Engineering, Faculty of Engineering, Computing and Mathematics,
The University of Western Australia, Australia

ARTICLE INFO

Keywords: Hybrid RuDSTC Rubberised concrete Axial loading Strain enhancement Ductility

A B S T R A C T

Rubberised concrete formed by using recycled scrap tyre chips as the substitution for natural aggregates, has recently emerged as an important research topic [Code a1]. Though it conserves the mineral aggregates, it is associated with reduced compressive strength [Code a1]. Different confinement techniques with fiber-reinforced polymer (FRP) wrapping and steel have been commonly used to restore the lost strength that also provided some other benefits such as enhanced ductility and energy dissipation capacity. [Code a1] In this paper, a novel hybrid double-skin tubular column termed as “Hybrid RuDSTC” consisting of rubberised concrete, filament wound circular CFRP tube, and cold-formed circular steel tube was developed and experimentally explored to evaluate its performance under axial load [Code a3]. The parameters of the experimental investigation were void ratio, slenderness ratio, and percentage rubber replacement. [Code a3] Results showed that the novel Hybrid RuDSTCs can provide a promising sustainable solution with greater strain capacity compared to their unconfined counterparts. [Code a4] Better strain and enhanced ductility of the hybrid RuDSTCs compared to non-rubberised hybrid DSTCs enable their use in seismic prone regions and mining infrastructure. [Code a5]

1. Introduction

Scrap tyre has been used in the form of rubber aggregates in a promising sustainable concrete termed as rubberised concrete. The disposal of waste tyres has become a huge burden in the landfills every year all over the world. Rubber aggregates as a partial replacement of natural aggregates have drawn attention from researchers in recent years[1–3]. The use of rubber aggregates in concrete has shown to improve seismic and impact

resistance, compressive strain, ductility, and damping potential [4–7,20]. However, rubberised concrete has been reported to impart reduced axial capacity compared to normal concrete. To negate this effect, several confinement solutions have been suggested by researchers. Fig. 1 indicates different types of confined rubberised concrete columns. The variations of confined rubberised concrete columns depends on the cross sectional geometry, material properties of inner and outer tubes, type and strength of concrete, confinement type and aggregate replacement type and ratio of rubber aggregates. Fig. 1 elaborates several types of confinement materials used till date. The confinement provided to rubberised concrete with outer steel or Fiber-reinforced polymer (FRP) tubes developed by wet layup method of FRP sheets are referred to as single skin column [3,5,8,9]. In actively confined rubberised columns, the external confining pressure is exerted by hydrostatic pressure[6]. The double skin tubular column provides confinement with two tubes and rubberised concrete is cast between both the tubes. Several forms of double-skin tubular columns have been explored by researchers in the recent decades which include rubberised concrete filled double skin steel tube (RuCFDST)[7,10]and Hybrid DSTC (double skin tubular column) with outer FRP wrapped tube and inner steel tube with rubbercrete[11]. Both the types have been reported to provide excellent corrosion resistance, ductility and energy dissipation capacity. Yu et al. [10] recommended that the hybrid double skin column to be suitable for mining infrastructure, while several researchers recommended its use in seismic prone regions [11–13].

In the present study the authors develop an innovative hybrid rubberised double-skin tubular column termed as “Hybrid RuDSTC” having a filament wound circular CFRP outer tube and an inner circular steel tube and the gap between the tubes filled with rubberised concrete. This innovative hybrid column combines the benefits of all four

* Corresponding author.

E-mail address: sabrina.fawzia@qut.edu.au (S. Fawzia).

Available online 14 August 2021

02638223/© 2021 Elsevier Ltd. All rights reserved.

materials; rubber, CFRP, steel and concrete. In most of the previous studies on rubberised columns, FRP sheet wraps were used. The use of

Table 1

Specimen details.

the filament wound CFRP tube in this novel hybrid RuDSTC enables a “ready to use” formwork and provides enhanced longitudinal and lateral strengths. This tube has been used to form several single and double skin columns[14–16]. However, their use in combination with steel and rubberised concrete is novel to the best of the knowledge of the authors.

type	D_o (mm)		t_o (mm)	D_i (mm)		t_i (mm)	
1 C-I60-00	CFRP	152	2.5	60.3	3.6	0%	
2 C-I60-15	CFRP	152	2.5	60.3	3.6	15%	
3 C-I60-30	CFRP	152	2.5	60.3	3.6	30%	
4 C-I101-00	CFRP	152	2.5	101.6	5	0%	

5 C-I101-15 CFRP	152	2.5	101.6	5	15%
6 C-I101-30 CFRP	152	2.5	101.6	5	30%
7 CL-I60-00 CFRP	152	2.5	60.3	3.6	0%
8 CL-I60-15 CFRP	152	2.5	60.3	3.6	15%
9 CL-I60-30 CFRP	152	2.5	60.3	3.6	30%

In this paper the response of the innovative hybrid RuDSTCs, both stub and slender, are experimentally tested under axial loads. The parameters for experimental investigation are the void ratio, slenderness ratio and the percentage of rubber replacement ratio by weight. This column is expected to provide excellent ductility and increased strain capacity and can be effectively used as a sustainable solution in seismic regions, mining infrastructure and in columns vulnerable to vehicular impacts.

Sl no.

Specimen ID

FRP

tube

Outer FRP tube properties
Inner steel tube properties
Rubber replacement

1. Specimen Details

Six stub hybrid RuDSTCs with two different void ratios and three slender hybrid RuDSTCs were prepared and tested in this study. For material testing, two CFRP filament-wound tubes, four circular hollow sections (CHS) steel tubes and nine concrete cylinders (three samples for each batch of 0%, 15%, and 30% rubberised concrete) were tested. Steel coupons were also prepared from CHS tubes according to AS1391 and tested to determine the mechanical properties of steel through tensile testing. The hybrid RuDSTC specimens details are given in Table 1. D_o and D_i represent the outer and inner diameters respectively while t_o and t_i represent the thicknesses of the outer filament wound CFRP tube and inner steel tube respectively. The specimens can be divided into three groups with two groups of stub columns and one group of slender columns. The first group has hybrid RuDSTCs with void ratio (ratio of inner steel tube diameter to outer CFRP tube diameter) 0.40 and the second group has thicker and wider diameter steel tube giving a void ratio of 0.67.

The length of all the stub columns was 300 mm. The third group of columns has similar cross-sections as the first group, but with a length of 1000 mm indicating the height to diameter ratio as 6.57. The specimens were labeled as: “C” for stub column and “CL” for slender column, “I” for diameter of the inner steel tube and % for amount of rubber replacement. For example, C-I60-15 indicates a stub hybrid RuDSTC with CFRP filament wound tube, inner steel tube of diameter 60.3 mm and 15% rubberised concrete.

1.

Preparation of Specimen

3.1. Rubberised concrete mix design

The maximum aggregate size was selected as 10 mm such that it was less than half of the interface gap between the tubes. Three different sizes of aggregates namely 10 mm, 7–10 mm, and 1–4 mm were used. The fine sand of grain size of 0.2–6 mm was used. Normal concrete with no rubber aggregates was termed as control concrete. The other two concrete types were 15% and 30% rubberized concrete with rubber replacing both fine and coarse aggregates. The design strength of the control concrete was 50 MPa. General-purpose Portland cement conforming to AS 3972 [13] was selected as the binding material.

To replace both fine and coarse aggregates, 1–5 mm and 7–10 mm rubber aggregates obtained from scrap tyre rubber were used. Fig. 2

represents the gradation curve of the selected aggregates. The rubber aggregates were received from the manufacturer as 1–5 mm and 5–10 mm rubber granules. The desired sizes of rubber aggregates were obtained through sieve analysis conforming to AS3638.

The mix design adopted for control concrete was 426 kg/m³ of cement, 444 kg/m³ of 10 mm aggregates, 306 kg/m³ of 7 mm aggregates, 130 kg/m³ of aggregates <4 mm, 843 kg/m³ of sand, and 205 kg/ m³ of water. The water-cement ratio was 0.48. The material content for rubberised concrete was calculated from the control mix based on the percentage of rubber replacement by weight.



Fig. 1. Different types of Confined Rubberised Concrete Columns.




Fig. 2. Gradation Curve of aggregates.

3.2. Formation of the novel hybrid RuDSTC

Formation of the novel hybrid RuDSTC required careful planning to make all the individual components come together and form an integrated composite. The steps below were followed to prepare the specimens.

Step 1: Welding of the inner steel tube with the bottom plate The inner tubes of the hybrid columns were C250LO grade CHS black pipe compliant with AS1074/1163[17] fabricated by the manufacturer in the desired length required for this test from a 6.5 m long tube. The inner steel tube was tack welded at the center of a 25 mm thick steel plate of 250 mm diameter, on a marked circle, and welded at one side only to work as a base plate to facilitate the casting of concrete as shown in Fig. 3. Care was taken to ensure that the steel tube is vertical with the base plate and that both centers were coincident.

Step 2: Attachment of strain gauges to the inner steel tube The layout of the strain gauges is given in Fig. 4. Strain gauges were labelled as “SGA” to indicate those in the axial direction and as “SGL” to indicate those in the lateral direction. Strain gauges were attached at the mid-height of the stub columns and at three equal intervals in the slender columns starting at 250 mm from the top. As these strain gauges were supposed to be embedded in concrete, special precautions were adopted as per the suggestions of the strain gauge manufacturers. The locations of strain gauges on the steel tube were determined and any rust or dirt in those locations was removed with sandpaper. The surface was made clean with acetone and gauges were attached to the prepared steel tubes using Cyanoacrylate adhesive.

 A wax coating was first applied to the strain gauges to prevent the cement grout into strain gauges and to ensure the insulation between the steel tube and electric wires. Layers of self-bonding tape, vinyl tape, and another layer of bonding tape were then applied in that order to protect the

strain gauges from the surrounding moisture and to prevent the aggregate crushing the attached strain gauges. Section A shown in the Figure above is located at the midsection of the columns and the arrangements of strain gauges for both stub and slender columns are similar in which one axial and two lateral strain gauges 180° apart were attached to the steel tubes. At sections B and C, one axial and one lateral strain gauge were attached to the steel tube of the slender column. Finally, the strain gauges wires were labelled for identification.

Step 3: Drilling holes in the CFRP tube for the strain gauge wires and centering of tubes Filament wound CFRP tubes of 152 mm diameter and 2.5 mm thickness made with carbon fibers were used in this study. 20%, 40%, and 40% fibers were oriented at the angles of 15°, 40°, and 75° with the longitudinal axis of the tube. Two very tiny holes that would have negligible effects (on the testing) were drilled on the CFRP tubes at the locations of 70 mm from the top and 180 degrees apart to take out the wires of the strain gauges. For slender columns, two additional holes of the same size were drilled at the bottom. A special steel spider shown in Fig. 5 was fabricated by the Design and Manufacture Center (DMC) of QUT, as a centering device for the both steel and CFRP tubes. The spider had three arms, each with two adjustable legs. The inner three legs were first attached to the steel tube, after which the CFRP tube was placed maintaining the same distance along the spider arms. At this stage, the three outer legs were attached to the CFRP tube with screws. After centering, the CFRP tubes were attached to steel plates using Sikaflex-111 multipurpose adhesive and sealing agent. The strain gauge wires along with the labels were then safely taken out through the holes.

Step 4: Rubber pre treatment The rubber particles, which were to be used as aggregates, were thoroughly washed with tap water to remove dirt and oil from their surface as their presence can hinder the bond strength at the cement-rubber interface. The rubber aggregates were then soaked in water for a duration of 24 h after which they were separated from water and dried in the air until their outer surface was adequately dry as shown in Fig. 6. These semi saturated rubber aggregates were used in the concrete mix, to ensure a stronger bond between rubber and concrete. The water-soaked by

rubber particles was calculated and deducted from the water used for mixing the concrete.

Step 5: Preparation of rubberized concrete Due to the tendency of rubber aggregates to segregate and float, the mixing technique recommended by Elchalakani [18] was followed which involves the following steps: (1) mix the dry aggregates for one minute, (2) add 10% of the mixing water to the dry aggregates and to the rubberized concrete (rubber is added in this step), (3) add the cement and mix for one minute, (4) add half of the remaining (90%) mixing water and mix for one minute, (5) add the final amount of 45% of water and mix for one minute. The slump was checked in this stage. To facilitate the casting of concrete in the narrow space between the tubes, the slump was chosen as 150–170 mm. Superplasticizer was added at a rate of 250–300 ml per cubic meter of concrete to achieve a desirable slump.



Fig. 3. Welded inner steel tube at the center of the steel base plate and sealed strain gauges.



Fig. 4. Layout of strain gauges.



Spider for centering Strain gauge wires CFRP tube glued with Steel base plate Fig. 5. Centering of CFRP and steel tube.



Step 6: Casting of concrete
Fig. 6. Rubber pre-treatment.

tamp the concrete. Three rectangular plates were tack welded to the


 Concrete casting is the most important and challenging task in this project. The gap between the tubes is very narrow and the wires from the strain gauges pass across these gaps. Before casting, the inner steel tube was covered with a plastic sheet to avoid any concrete entering the inner tube. Concrete vibrator cannot be used as the rubber particles are light and the vibration can cause the rubber particles to float to the top and hinder a homogeneous mix. A steel rod was instead used to manually base plate in each of the slender column specimens to provide support to the outer CFRP tube during movement after casting. These steel plates were removed after curing without affecting the specimen geometry. Nine hybrid RuDSTC specimens and nine concrete cylinders with 0%, 15%, and 30% of rubber concrete were cast. After casting, the column specimens as well as concrete cylinders were covered with a thin plastic sheet to prevent the loss of moisture from the concrete as shown in



Fig. 7.

Step 7: Curing of specimens
Fig. 7. Rubberised concrete preparation and casting.

as shown in the Fig. 4. To prevent premature failure of the outer CFRP tube, three-ply of unidirectional MBrace Fib 300/50 carbon fiber

All hybrid RuDSTC specimens and concrete cylinders were kept in the moist room at 21 °C temperature until 21 days to ensure proper curing. After that, the specimens were shifted from a moist room to a shaded area until the testing day.

Step 8: Levelling specimen top surface After 3 weeks, longitudinal gaps were observed in the concrete of the hybrid specimens due to shrinkage. Rapid hardening adhesive mortar Sikadur 31/41 was used to fill the gaps and allowed to remain for 24 h so that the concrete surface could be flush with the CFRP and steel tube at the top. However, to ensure a smooth and flat surface for applying a uniform compression loading, the top surfaces of the specimens were ground using a high strength concrete grinder.

Step 9: Strain gauges on CFRP tube and CFRP wrapping Two sets of axial and lateral strain gauges were attached to each CFRP tube in the stub columns at 180° apart and in parallel to the strain gauges attached to the steel tubes. For the slender columns, fifteen strain gauges were attached in the axial and lateral directions in three sections sheets of 30 mm width were wrapped around the specimens at the top and bottom by Mbrace saturant with two-parts of epoxy resin with an overlapping length of 100 mm and cured for 7 days.

1. Test Set Up

The specimen was placed on the lower compression platen concentrically with respect to the upper and lower compression platen as shown in Fig. 8. In order to provide a uniform compression, a 60 mm thick steel plate was placed at the top of the specimen at the time of testing. The load was applied through the load cell by bringing the 60 mm plate in close contact to the load cell. A uniform compression loading was applied on the specimens at a displacement rate of less than one mm per minute. A universal data acquisition system with a 500 Tonne load cell were used.

A string pot was mounted on the top-loading plate to measure the overall axial displacement of the column. All the strain gauges were

String pot

60 mm thick steel plate

Specimen

Ram Load cell

 Camera

Lower compression platen

Data acquisition system

Fig. 8. Test set up.

connected with the data acquisition system and checked before applying the load. A high-speed camera with an efficiency of five shots per second was used to capture photos.

4.1. Material testing

4.1.1. Steel

Two types of cold-formed CHS tubes were tested under compression to ascertain the material property parameters as listed in Table 2. ST1 and ST2 tubes were identical having 60.3 mm diameter and 3.6 mm thickness. ST3 tube had 101.6 mm diameter and 5 mm thickness. The length of ST1, ST2, and ST3 tubes was 300 mm similar to the stub columns. Tube ST4 had similar cross-sections as ST1 and ST2 but had a length of 1000 mm to replicate the behavior of the inner steel tube of the slender column. The tubes were tested in the universal testing machine keeping the same test set up as shown in Fig. 8. The dimensions of the different tubes are listed in Table 2.

Identical tubes ST1 and ST2 showed similar load–displacement curves (Fig. 9) and failure mode was global buckling along with diamond mode. The thicker tube ST3 showed elephant foot buckling mode after failure. Behaviour of the longer tube ST4 was also dominated by global buckling failure mode.

The results of the mechanical properties of the tubes are listed in Table 2. As per Table 2, the maximum squash load 590 kN was recorded for the ST3 tube and the maximum strain was observed for ST1 as 64,642 microstrains. Static tensile coupon testing was conducted pertaining to AS1391 to obtain the mechanical properties of the steel tubes. The modulus of elasticity obtained from the coupon test is 193 GPa.

4.1.2. Filament wound CFRP tube

Two identical hollow CFRP tubes namely CFRP-1 and CFRP-2 of 152 mm diameter and 300 mm length were tested under compression loading. Fig. 10 shows the load–displacement curves of the tubes.

The maximum squash load for the identical tubes on average was 167 kN. CFRP-2 tube underwent greater displacement before failure although both the tubes had a similar modulus of elasticity calculated as 24 GPa in the longitudinal direction of the tube. Failure of both tubes occurred only at the top cross-section leaving the rest of the tube un-affected. Failure mode of the bare CFRP tube can be observed in Fig. 11.

4.1.3. Concrete

As per AS1012.8 (2014), nine concrete cylinders (three for each concrete type) of 100 mm diameter and 200 mm height were cast for control concrete, 15% rubberised concrete, and 30% rubberised concrete. These cylinders and the hybrid column specimens were cast and tested on the same day. The average values of the densities of the cylinders obtained before testing were 2248 kg/m³, 2019 kg/m³, 1731 kg/m³ respectively for 0%, 15% and 30% rubberised concrete. The average compressive strengths obtained from the test were 50.15 MPa, 24.86 MPa, and 9.75 MPa for 0%, 15%, and 30% rubberised concrete respectively. The compressive strength of 15% rubberised concrete is within the range of 20–25 MPa which can be effectively used in structural applications. The compressive strength decreased by 50% and 80% respectively for 15% and 30% rubber replacement by weight.

Table 2

Mechanical properties of steel hollow tube.




 Fig. 9. Axial load–axial displacement curves of hollow steel tubes.



Fig. 10. Axial load–displacement plots of CFRP hollow tubes.

1. Experimental Observations and Results

The following observations were made from the results of testing the hybrid RuDSTC specimens.

5.1. General

Fig. 12 indicates the axial stress-axial strain curves of all the specimens tested in this investigation. The readings of compressive loads and corresponding displacements were recorded until the final rupture of the CFRP tube occurred with a loud bang. The rubberised columns showed lower axial stress capacity compared to the control specimen for all three groups of specimens. However, most of the rubberised columns showed greater axial strain at failure. The concrete enclosed with the filament wound CFRP tube showed an increase in axial stress and strain even after the initiation of the first crack associated with a sharp

Tube ID	Diameter (mm)	Thickness (mm)	Length (mm)	Squash load on the tube (kN)	Maximum strain ($\mu\epsilon$)	Coupon test results	
						yield stress (MPa)	ultimate strength (MPa)
ST1	60.3	3.6	300	255	64,642	331	377
ST2	60.3	3.6	300	260	61,833	331	377

ST3	101.6	5.0	300	590	62,760	345	387
ST4	60.3	3.6	600	213	10,142	331	377



Concrete cylinders after testing Deformed hollow steel tubes

Deformed CFRP tube

Fig. 11. Deformed specimens after material testing.



Fig. 12. Axial stress and nominal axial strain curves (a) C-I60, (b) C-I101, and (c) CL-I60.

snapping sound which indicates damage in resin. The occurrence of the first cracks was delayed for rubberised specimens as compared to the control specimens. Cracks in the filament wound tube can be observed with a slight drop in the stress–strain curve. As the loading progressed, the cracks in the CFRP tube increased due to the lateral pressure exerted by the enclosed concrete, which appeared mostly in the top, and bottom one-third region for all rubberised and non-rubberised stub columns as can be seen in Fig. 13. The axial stress–strain capacity of slender columns was less than stub columns, which may be due to the global buckling phenomenon that was more pronounced in rubberised columns than the control concrete columns.

After the tests, all the deformed specimens, shown in Fig. 14, were carefully examined. Spring back phenomenon was observed in the rubberised

column, which indicated that the rubber particles pushed the concrete up during the unloading stage. Maximum spring back of 3 mm was observed for the C-I60-30 column and a minimum 0.5 mm for the C-I101-30 column.

The observation made on the inner steel tube indicated prominent internal buckling in the control rubberised columns. This can be best observed on C-101 columns with a larger internal diameter and it occurred due to the increased concrete pressure under increased load.

However, buckling of the internal tube was very minimal for rubberized columns mainly due to the deformability of rubber aggregates indicating effective confinement provided by the rubber concrete, securing the inner steel tube, and enhancing the ductile behavior of the hybrid RuDSTCs. The CFRP tube was damaged due to the combined actions of axial and hoop stresses. More localized damage was observed in slender columns than in the stub columns.

5.2. Effect of rubber aggregates on axial load-

Eight strain gauges in the stub columns and fifteen strain gauges in the slender columns were installed. Almost all of them functioned well, though a few on the steel tubes had become faulty. Fig. 13 depicts the load vs strain plots of the rubberised specimens obtained from the load cell and strain gauges installed in these specimens. At the early stages, the load strain curves are almost vertical and imply near uniform but small values in the strains.

For the specimen with 15% rubberized concrete, the initial strains in the steel and CFRP tubes were the same for both the stub and slender columns but as loading increased axial strains in the steel tube obtained from SGA1 were greater than those in the CFRP tube. As the CFRP tube



Fig. 13. Axial load–strain plots of RuCFWDSTCs; (a) C-I60-15, (b) C-I101-15, (c) CL-I60-15(d)C-I60-30, (e) C-I101-30, (f) CL-60-30.



Fig. 14. Deformed RuCFWDSTC columns after testing (a) C-I60 columns, (b) C-I101 columns and (c) CL-60 columns.

was inactive until the lateral pressure from the expanding concrete occurred, the lateral strains in steel tube obtained from SGL1 and SGL2 are greater than those in the CFRP tube indicated by the relatively smaller values from SGL3 and SGL4. For the C-I101-15 column, strain gauge pairs located 180° apart SGL1 and SGL2 on steel and SGL3 and SGL4 on CFRP tube showed good agreement in strain readings indicating uniform strain developments along the circumference of the circular hybrid column.

For the slender column CL-I60-15, the variations in the strain gauge readings pertaining to the hoop and axial strains started early due to the global buckling phenomenon. The lateral strain values of the inner steel tube and CFRP tube at the midzone were higher than those at the top and bottom for both the tubes that match the buckle shape. Significant axial resistance having a value close to that of a steel tube was provided by the CFRP tube as can be observed from their axial strains and demonstrate the axial capacity of the filament wound CFRP tube, unlike the FRP sheet wrapping. For 30% rubberized columns, as can be seen from Fig. 13, the load vs strain curves of the stub and slender columns are similar to those in the 15% rubberized column.

A summary of the key test results is presented in Table 3, which indicates peak values of stresses, and strains were effectively delayed due to the use of rubber aggregates. The decrease in the axial capacity (due

Table 3

Summary of the key test results

to the rubber aggregates replacing the normal aggregates) was found to be in the range 4.50 to 47.52% for stub columns and 18.73 to 49.98% for the slender columns. However, the strain capacity at peak load in the stub columns increased to 43.42% for 15% rubberized concrete and 41.60% for 30% rubberised concrete. The ultimate strain increase for stub columns was 27.32% for 15% and 37.12% for 30% rubberised concrete respectively. The slender column with 15% rubberized concrete showed better performance of strain increase than that with 30% rubberised concrete

5.3. Effect of void ratio

To compare the effect of void ratio on overall performances of the specimens, axial stress and axial strain curves of C-I60 (void ratio 0.40) columns and C-I101 (void ratio 0.67) columns were compared as shown in Fig. 15. Stress drop was observed for the control specimen with a larger void ratio similar to the findings of Zhang et al.[16] and Fanggi et al.[19]. However, for the smaller diameter control specimen, no stress drop was observed. Hybrid columns with a larger void ratio and thicker inner tube showed greater strain capacity with the increase of rubber percentage. Stiffness of the second branch of the stress–strain curve decreases resulting in a more moderate plateau that indicates

Specimen ID Peak Stress

(MPa)

Peak strain ($\mu\epsilon$)

Ultimate axial strain ($\mu\epsilon$)

Axial capacity (kN)

Capacity decrease %

Ultimate strain increase %

Peak strain increase %



C-I60-00 110.44 32,824 34,005 1692 – – – C-I60-15 83.95 35,445 35,466
1286 23.98 4.3 7.99

C-I60-30 57.96 34,448 46,263 888 47.52 36.05 4.95

C-I101-00 148.48 30,000 39,500 1505 – – – C-I101-15 141.80 43,027
50,293 1437 4.5 27.32 43.42

C-I101-30 111.31 42,500 54,160 1128 25.03 37.11 41.67

CL-I60-00 93.50 22,390 22,390 1432 – – – CL-I60-15 75.99 25,400 26,690
1164 18.73 19.21 13.44

CL-I60-30 46.77 22,992 23,060 716 49.98 2.99 2.69



more ductile behavior.

5.4. Effect of height to diameter ratio

Fig. 15. Effect of void ratio on axial stress and axial strain.

5.5. Ductility index

Ductility is an important parameter to compare the behaviour of the columns. It is represented by the ductility index (DI). There are two

Stress–strain curves of C-I60 columns and CL-I60 columns were compared in Fig. 16. All the columns of these two groups have similar cross-sections. However, the specimen slenderness was calculated based on the ratio of the height to the diameter that was 1.97 for stub columns and 6.57 for slender columns. Examining the results, it was evident that the longer columns underwent stress drops before reaching the peak stress and both maximum stress–strain capacity of slender columns were less than stub columns.

This may be due to the effect of global buckling. However, for stub columns, the strain increased with an increasing percentage of rubber from 0 to 30%, whereas, for slender columns, the strain of 30% rubberised column was less than 15% rubberised column.

approaches to calculate DI namely displacement-based DI and equivalent energy-based DI. In this paper, DI was calculated from the load–displacement plots similar to the approach adopted by Duarte et al.

[5]. The ratio $A1/A2$ was used in energy-based ductility index calculation, where $A1$ indicates the irrecoverable plastic energy and $A2$ indicates recoverable elastic energy calculated at peak stress. A higher value of DI ensures better ductile behaviour. Fig. 17 compares the ductility index of all specimens investigated in this study. The ductility index of hybrid columns ranges from 2.74 to 7.07.

Ductility of all three groups of the columns increased with increased rubber percentages. However, columns with greater void ratio and thicker inner tube showed better ductility amongst all.



Fig. 16. Effect of height to diameter ratio on axial stress and axial strain.



1. Conclusions

Fig. 17. Ductility indices of the hybrid RuDSTCs.

columns with better strain enhancement and ductility compared to non-rubberised hybrid DSTCs suitable for use in seismic prone re-Through this experimental study, the behavior of the novel hybrid RuDSTC was investigated for the first time. From the experimental results, the filament wound CFRP confinement had proven to be effective and its use in combination with rubberised concrete has indicated promising results with enhanced peak axial strain, maximum strain capacity and ductility with increased rubber content under axial compressive loading. The major observations of the study are summarized below:

1. The strength of control concrete decreased by 50% and 80% respectively for replacement of both the fine and coarse aggregates by 15% and 30% rubber respectively. However, the use of hybrid double skin confinement provided by filament wound CFRP and steel tubes showed that the capacity decrease of hybrid column was 4.50% to 23.98% for 15% rubberised stub columns and 18.73% for 15% slender column. For 30% rubberised concrete, the capacity decrease was 25.03% to 47.52% for stub columns and 49.98% for the slender column. It can be seen that the hybrid confinement was effective in partially restoring the concrete strength when using rubber aggregates.
2. The stress–strain plots of hybrid RuDSTCs indicated bilinear

behavior similar to those of non-rubberised columns associated with reduced capacity but delayed peak value of ultimate axial strain. Strain capacity of rubberised columns showed better results compared to the control specimens. The strain capacity at the peak was increased to 43.42% for 15% rubberized concrete and 41.6% for 30% rubberised concrete. The

ultimate strain increases were 27.32% and 37.12% for specimens with 15% and 30% rubberised concrete respectively.

1. Prominent inward buckling of the inner steel tube was observed for non rubberised columns that were absent in rubberised columns. This indicates the inner steel tubes were well protected by rubberised concrete and filament wound tube to ensure more ductile behaviour. The spring back phenomenon was observed in rubberised columns with 30% rubber.
2. Increased void ratio showed enhanced axial stress and strain capacities of the columns. Longer columns showed reduced capacity and strain compared to the stub columns with similar cross-section due to global buckling.
3. The ductility of hybrid RuDSTC increased with increased rubber content. The second group of columns with thicker and wider steel tubes showed more ductile behavior compared to all other columns.
4. The novel hybrid RuDSTCs can be a promising sustainable solution with greater capacity compared to unconfined rubberised concrete

gions and mining infrastructure.

Declaration of Competing Interest

The authors declare that they have no known competing financial interests or personal relationships that could have appeared to influence the work reported in this paper.

Acknowledgements

The authors wish to thank the technical staff, Mr. Frank De Bruyne, Mr. Glenn Atlee, Mr. Barry Hume, Mr. Cameron Creevy, Mr. Zeph Kadel for their assistance in conducting the experimental study reported in this research at the Banyo Pilot Plant Precinct of Queensland University of Technology (QUT), Mr. Greg Patterson for training and providing support

in material testing and Design and Manufacture Centre (DMC) of QUT. The authors also wish to thank the School of Civil Engineering& Built Environment at the Queensland University of Technology (QUT), Australia for the financial support for the experimental work reported in this study.

Data availability statement

The raw/processed data required to reproduce these findings cannot be shared at this time as the data also forms part of an ongoing study.

References

- [1] [Abendeh R, Ahmad HS, Hunaiti YM. Experimental studies on the behavior of concrete-filled steel tubes incorporating crumb rubber. J Constr Steel Res 2016; 122:251–60.](#)
- [2] [Bompa DV, Elghazouli AY. Stress–strain response and practical design expressions for FRP-confined recycled tyre rubber concrete. Constr Build Mater 2020;237.](#)
- [3] [Chan CW, Yu T, Zhang SS, Xu QF. Compressive behaviour of FRP-confined rubber concrete. Constr Build Mater 2019;211:416–26.](#) [4] [Dong M, Elchalakani M, Karrech A, Hassanein MF, Xie T, Yang Bo. Behaviour and design of rubberised concrete filled steel tubes under combined loading conditions. Thin-Walled Struct 2019;139:24–38.](#)
- [5] [Duarte APC, Silva BA, Silvestre N, de Brito J, Júlio E, Castro JM. Tests and design of short steel tubes filled with rubberised concrete. Eng Struct 2016;112:274–86.](#) [6] [Gholampour A, Fallah Pour A, Hassanli R, Ozbakkaloglu T. Behavior of actively confined rubberized concrete under](#)

[cyclic axial compression. J Struct Eng 2019; 145.](#) [7] [Khusru S, Fawzia S, Thambiratnam DP, Elchalakani M. A parametric study: High performance double skin tubular column using rubberised concrete. Compos Struct 2020;235:111741.](#) [8] [Bompa DV, Elghazouli AY. Behaviour of confined rubberised concrete members under combined loading conditions. Mag Concr Res 2019;1–55.](#)

[9] [Hassanli R, Youssf O, Vincent T, Mills JE, Manalo A, Gravina R. Experimental study on compressive behavior of FRP-confined expansive rubberized concrete. J Compos Constr 2020;24\(4\):04020034.](#) [10] Yu T, Remennikov A. Hybrid double-skin tubular members for sustainable mining infrastructure. 2013. [11] [Wong YL, Yu T, Teng JG, Dong SL. Behavior of FRP-confined concrete in annular section columns. Compos B Eng 2008;39\(3\):451–66.](#) [12] [Abdelkarim OI, ElGawady MA. Analytical and finite-element modeling of FRP- concrete-steel double-skin tubular columns. J Bridge Eng 2015;20:B4014005.](#) [13] [Huang L, Yin P, Yan L, Kasal B. Behavior of hybrid GFRP–perforated-steel tube-encased concrete column under uniaxial compression. Compos Struct 2016;142: 313–24.](#)

[14] [Li YL, Zhao XL, Singh Raman RK. Mechanical properties of seawater and sea sand concrete-filled FRP tubes in artificial seawater. Constr Build Mater 2018;191: 977–93.](#)

[15] [Li YL, Zhao XL, Singh RKR, Al-Saadi S. Experimental study on seawater and sea](#)

[sand concrete filled GFRP and stainless steel tubular stub columns. Thin-Walled Struct 2016;106:390–406.](#)

[16] [Zhang B, Teng JG, Yu T. Compressive behavior of double-skin tubular columns with high-strength concrete and a filament-wound FRP tube. J Compos Constr 2017;21.](#) [17] Standard A. Cold-formed structural steel

hollow sections. AS 1163: Standards association of Australia; 2016. [18] [Elchalakani M, Hassanein MF, Karrech A, Fawzia S, Yang Bo, Patel VI. Experimental tests and design of rubberised concrete-filled double skin circular](#)

[tubular short columns. Structures 2018;15:196–210.](#)

[19] [Louk Fanggi BA, Ozbakkaloglu T. Compressive behavior of aramid FRP–HSC–steel double-skin tubular columns. Constr Build Mater 2013;48:554–65.](#) [20] Khusru S, Fawzia S, Thambiratnam DP, Elchalakani M. Confined rubberised concrete tubular column for high-performance structures – Review. Constr Build Mater 2021;276(122216):1–16.<https://doi.org/10.1016/j.conbuildmat.2020.122216>. 122216. In this issue.